Journal Pre-proofs

Research paper

Design and Synthesis of Three Fe(III) Mixed-ligand Complexes: Exploration of Their Biological and Phenoxazinone Synthase-Like Activities

Mohammed Ismael, Abdel-Mawgoud M. Abdel-Mawgoud, Mostafa K. Rabia, Aly Abdou

PII: S0020-1693(19)31609-3
DOI: https://doi.org/10.1016/j.ica.2020.119443
Reference: ICA 119443

To appear in: *Inorganica Chimica Acta*

Received Date: 23 October 2019
Revised Date: 22 December 2019
Accepted Date: 11 January 2020

Please cite this article as: M. Ismael, A.M. Abdel-Mawgoud, M.K. Rabia, A. Abdou, Design and Synthesis of Three Fe(III) Mixed-ligand Complexes: Exploration of Their Biological and Phenoxazinone Synthase-Like Activities, *Inorganica Chimica Acta* (2020), doi: https://doi.org/10.1016/j.ica.2020.119443

Design and Synthesis of Three Fe(III) Mixed-ligand Complexes: Exploration of Their Biological and Phenoxazinone Synthase-Like Activities

Mohammed Ismael*, Abdel-Mawgoud M. Abdel-Mawgoud, Mostafa K. Rabia and Aly Abdou
Chemistry Department, Faculty of Science, Sohag University, Sohag 82524, Egypt

Abstract

New Fe(III) complexes with mixed ligands based on 1-{(E)-[(4-methylphenyl)imino]methyl}-2-naphthol (HN) as primary ligand and secondary co-ligand of O-hydroxy quinolone (HQ), 2-(1H-benzimidazol-2-yl)phenol (HB) and 2-(4,5-diphenyl-1H-imidazol-2-yl)phenol (HI) had been isolated and characterized. The isolated complexes had 1:1:1 ratio for Fe(III):ligand:co-ligand with one chloride and one water molecule coordinated to the Fe-centre, suggesting octahedral structure around the Fe-center with the formula [Fe(Ligand)(co-ligand)(Cl)(H_2O)]. Theoretical calculations using density functional theory by B3LYP with LANL2DZ basis set had been done for two possible orientations of the ligand moieties around the Fe-center, to find out the most reliable coordination modes. Calculations include geometry optimization, molecular orbital description, and energy evaluation of trans- and cis- coordination modes of the chloride and water around the Fe-center. *In-vitro* antibacterial and antifungal properties of the isolated complexes have also been examined against pathogenic bacteria, *E. coli* (G^-), *B. cereus* (G^+), and *A. Fumigatus* fungi, by using broth microdilution and disc diffusion methods. The target compounds exhibited considerable growth inhibition against selected pathogenic microorganisms as antimicrobial candidates with low minimum inhibitory concentration (MIC). The complexes showed biomimetic phenoxazinone synthase-like activity for the aerial coupling oxidation of o-aminophenol (OAP) to phenoxazine-2-one (Phz), in acetonitrile (ACN) solution, with high turnover number (K_{cat}). Structure Activity Relationship (SAR) model was derived, using Multi-Linear Regression analysis, by correlation the practical biological (MIC) data with calculated chemical descriptors.

Keywords

Fe(III) mixed-ligand complexes, phenol-based Schiff base, imidazoles, *in-vitro* antimicrobial activity, DFT calculations, phenoxazinone synthase-like activity, Structure activity relationship.

1. Introduction

Transition metal based Schiff-base complexes play a key role in the field of biological aspects, and organic catalysis[1,2]. Design and synthesis of transition metal complexes incorporating a combination of Schiff-base ligand with N-containing heterocyclic ring are of great interest in view of the possibility of increases the variety in chemical structure and obtaining diverse structures with intriguing specificities.

In biology; imidazoles, benzimidazoles, and 2-hydroxy quinoline derivatives can be termed 'Master Key'[3] as it is the main important core in many categories of therapeutic reagents, e.g. anticancer[4], antimicrobial[5], anti-inflammatory[6], anticonvulsant, anti-diabetic[7], antihypertensive[8], anti-tubercular[9], antiviral[10] and anti-parasitic reagents[11], anti-oxidants, proton pump inhibitors, anti-coagulants, hormone modulators, CNS stimulants as well as depressants and lipid level modulators, etc. [3]. Therefore, introductions of imidazole, benzimidazole, 2-hydroxy quinoline as secondary co-ligand will significantly enhance the biological properties.

On the other hand, Phenoxazinone synthase, a multicopper metalloenzyme, plays a crucial role in the biosynthesis of actinomycin D through the oxidative coupling of a wide range of 2-aminophenols (OAPs) to phenoxazinone. Actinomycin D is one among the most potent antineoplastic agents, which is most effective against Wilms tumor, gestational choriocarcinoma, Ewing's Sarcoma, testicular cancer and ovarian cancer for some extent. This is due to the intercalation of phenoxazinone chromophore with DNA base-pairs followed by blocking the creation of RNA[12]. Research study on the catalytic oxidation of OAP to 2-amino-3H-phenoxazine-3-one (Phz) by metal complexes has considerable attraction for providing important information about bioinorganic reactions and mechanistic aspects in the organic transformation which may open a new avenue in molecular science.

In the present framework, three Fe(III) ternary complexes involving a Schiff base as the primary ligand, and N-containing heterocyclic ring as the secondary one, had been prepared and characterized. Additionally, antifungal, antibacterial properties, and catalytic activity towards the oxidative coupling of OAP had been investigated. Furthermore, density functional theory (DFT) calculations had been performed to ascertain the 3D structure of the complexes, and correlate experimental biological (MIC) and catalytic (K_{cat}) activity with the estimated chemical descriptors for SAR model generation.

2. Experimental

2.1. Reagents

Chemicals used in synthesis of ligands and their metal complexes including benzil (ADWIC, 99.0 %), 2-hydroxy-benzaldhyde (ADWIC, 99.0 %), p-toluidine (ADWIC, 99.0 %), 2-hydroxy-1-naphthaldehyde (Sigma-Aldrich, 98.0 %), O-phenylene-diamine (Sigma-Aldrich, 98.0 %), salicylic acid (ADWIC, 99.0 %), 8-hydroxyquinloine (Sigma-Aldrich, 98.0 %), 2-aminophenol (Sigma-Aldrich, 98.0 %), Iron(III) chloride hexahydrate (Sigma-Aldrich, 98.0 %), were used as received without further purification.

2.2. Physical Measurements

JENWAY model 6405 UV-Vis. spectrophotometer, BRUKER Avance 400 instrument, BRUKER FT-IR model 8101 in the region 4000-400 cm^{-1}, JENWAY conductivity meter, Bartington Susceptibility instrument model 4320, and BRUKER D8-ADVANCE, were used for the absorbance, NMR, FT-IR, Conductivity, Magnetic susceptibility, and powder-XRD, measurements respectively.

2.3. Synthesis of the ligands

Synthetic procedure of the subject ligands, HN, HB and HI ligands are listed in the Supplementary information.

2.4. Synthesis of the Fe(III) ternary complexes

An aqueous solution of the Iron(III) Chloride (2.0 mmol, 0.54 g in 10.0 H_2O) was added drop wise to a mixture of the phenol-based Schiff base ligand [HN (2.0 mmol, 0.522 g) in 8.0 ml ethanol] and the N-containing heterocyclic co-ligand [HQ (2.0 mmol, 0.290 g), HB (2.0 mmol, 0.420 g) or HI (2.0 mmol, 0.624 g) in 8.0 ml ethanol]. The reaction mixture was refluxed with stirring for about 8.0 h at 80 ^{o}C. Afterwards, the mixture was lifted overnight for slow solvent evaporation. The resulting product was collected, washed by water-ethanol (3:7) and finally purified, Scheme (1).

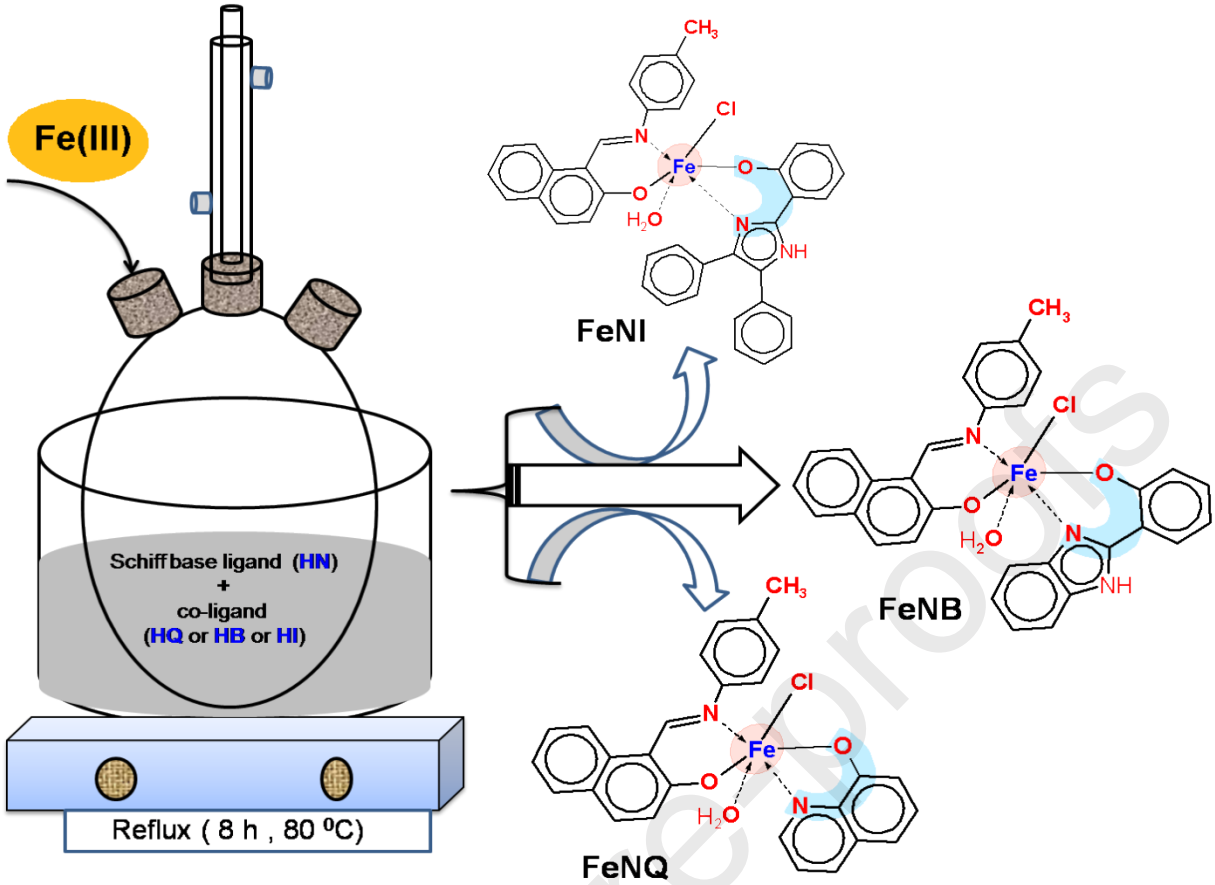

Scheme (1): Synthesis of the Fe(III) ternary complexes.

FeNQ complex: $[Fe(L)(Q)(H_2O)Cl].2H_2O$:

Color, dark brown, m.p. >300 ^{0}C, yield, 80%. Anal. Found (calc.) for ($C_{27}H_{22}ClFeN_2O_3$. $2H_2O$, 549.8 g/mol) (%): C, 58.06 (58.98), H, 4.10 (4.77), N, 5.57 (5.10), Cl, 6.89 (6.45), Fe, 10.45 (10.16). FT-IR, (υ, cm^{-1}): 3415 (H_2O), 3189 (-NH), 1555 (-CH=N), 1510 (-C=N), 1284 (C-O), 560 (M-O), 426 (M-N). UV-vis. (10^{-3} M acetonitrile solution, (λ_{max}, nm)): 360, 490 (n→π*, LMCT). Molar conductivity (10^{-3} M ethanol solution, (μ_v, $\Omega^{-1}.cm^2.mol^{-1}$)): 15.8 (Non-electrolyte nature). Magnetic moment (μ_{eff}, B.M): 1.91.

FeNB complex: $[Fe(L)(B)(H_2O)Cl].2H_2O$:

Color, dark brown, m.p. >300 ^{0}C, yield, 85%. Anal. Found (calc.) for ($C_{31}H_{25}ClFeN_3O_3.2H_2O$, 614.9 g/mol) (%): C, 59.82 (60.55), H, 4.01 (4.75), N, 7.13 (6.83), Cl, 5.04 (5.77), Fe, 9.85 (9.08). FT-IR, (υ, cm^{-1}): 3430 (H_2O), 3140 (-NH), 1580 (-CH=N), 1512 (-C=N), 1273 (C-O), 520 (M-O), 436 (M-N). UV-vis. (10^{-3} M acetonitrile solution, (λ_{max}, nm)): 320, 460 (n→π*, LMCT). Molar conductivity (10^{-3} M ethanol solution, (μ_v, $\Omega^{-1}.cm^2.mol^{-1}$)): 14.0 (Non-electrolyte nature). Magnetic moment (μ_{eff}, B.M): 1.93.

FeNI complex: $[Fe(L)(I)(H_2O)Cl].3H_2O$:

Color, dark brown, m.p. >300 ^{0}C, yield, 85%. Anal. Found (calc.) for ($C_{39}H_{31}ClFeN_3O_3$. $3H_2O$, 735 g/mol) (%): C, 63.06 (63.73), H, 4.48 (5.07), N, 5.16 (5.72), Cl, 5.14 (4.82), Fe, 7.18 (7.60). FT-IR, (υ, cm^{-1}): 3420 (H_2O), 3122 (-NH), 1585 (-CH=N), 1520 (-C=N), 1287 (C-O), 535 (M-O), 422 (M-N). UV-vis. (10^{-3} M acetonitrile solution, (λ_{max}, nm)): 340, 470 ($n\rightarrow\pi^*$, LMCT). Molar conductivity (10^{-3} M ethanol solution, (μ_v, $\Omega^{-1}.cm^2.mol^{-1}$)): 12.5 (Non-electrolyte nature). Magnetic moment (μ_{eff}, B.M): 1.97.

2.5. Density Functional Theory (DFT) Calculations

Geometry optimizations of the subject compounds in the gas phase were carried out at a gradient corrected DFT using hybrid correlation functional (B3LYP) combined with LANL2DZ basis set with effective core potential (ECP)[13], implemented in Gaussian 09 software[14]. The optimized structures and molecular frontier orbitals were visualized with GaussView 5.0 software.

To investigate the chemical reactivity of the optimized complexes, chemical descriptor parameters had been calculated including: energy gap $\Delta E = E_{LUMO} - E_{HOMO}$, electronegativity $\chi = -½ (E_{HOMO} + E_{LUMO})$, electronic chemical potential $\mu = ½ (E_{HOMO} + E_{LUMO}) = -\chi$, global chemical hardness $\eta = ½ (E_{LUMO} - E_{HOMO})$, global softness $\sigma = 1/2\eta$, global electrophilicity index $\omega = \mu^2/2\eta$, and nucleophilicity index $Nu = 1/\omega$, where E_{HOMO} and E_{LUMO} are the energies of highest occupied molecular orbital and the lowest unoccupied molecular orbital, respectively[15].

2.6. *In-vitro* exploration of antimicrobial activity

Antimicrobial activity of the free ligands and their Fe(III) complexes were *in-vitro* screened against pathogenic bacteria, *E. coli* (G^-), *B. cereus* (G^+), and *A. fumigatus* fungi. Broth microdilution[16] and disc diffusion methods[17,18] were applied for measuring the minimum inhibitory concentration (MIC, µg/mL) and the inhibition zone (IZ, mm), respectively.

The Petri dishes were filled by nutrient agar using Pour plate's protocol. Then, the nutrient agar medium was seeded with tested microorganisms (*E. coli* (G^-), *B. cereus* (G^+) and *A. fumigates*) in Petri dishes. Uniformed dices (5.0 mm diameter) of the subject compound with 100 µg/mL concentration were placed on the culture plates and incubated at 37 °C for 24 h. The antimicrobial activity was determined by measuring the diameter of the inhibition zone (mm).

2.7. Exploration of the Phenoxazinone synthase mimicking activity

To explore the ability of the Fe(III) complexes for coupling oxidation of OAP to Phz; 2.8 mL of 0.01 mol.dm^{-3} solution of substrate OAP was treated separately with 0.1 mL of 1 x 10^{-5} mol.dm^{-3} catalyst solution Fe(III) complex, and the volume was made to 3.0 mL by using acetonitrile, then a wavelength scan of the solution was recorded at a regular time interval of ten minutes, under aerobic conditions at room temperature (25 ^{o}C). The increase in the absorbance as a function of time around ≈ 430 nm, characteristic of the Phz, confirmed the phenoxazinone synthase mimicking activity.

2.7.1. Kinetics of Phenoxazinone synthase mimicking activity

In order to get further insight into the kinetics of penoxazinone synthase mimicking activity of the Fe(III) complexes; 0.1 mL of 1×10^{-5} mol.dm^{-3} of each catalyst Fe(III) complex was added to a series volumes of 1.8, 2.0, 2.2, 2.4, 2.6 and 2.8 mL of 0.01 mol.dm^{-3} OAP substrate. All these solutions were then made to 3.0 mL by using acetonitrile solvent, under aerobic conditions at room temperature. Raw data was taken as absorbance (A) at a regular time interval of ten minutes for a period of two hours. The product concentrations [Phz] at several reaction times were calculated from Beer-Lambert's law, $A_{430nm} = \varepsilon_{Phz} \times L \times [Phz]$, where $A_{430\,nm}$ is the Phz absorbance, ε_{Phz} is the molar extinction coefficient (1.093×10^4 cm^{-1} mol^{-1}.dm^3) [19], L is the length of the quartz cuvette (L = 1 cm) and [Phz] is the molar concentration of Phz (mol.dm^{-3}). The change in [Phz] is plotted against time (t, h). The initial rate values for the particular catalyst, at each substrate concentration were evaluated from the maximum slope (V_0 = d[Phz]/dt, mol.dm^{-3}.h^{-1}).

The initial rate values V_0 and product concentration [Phz] were used on the basis of Michaelis-Menten kinetics, Lineweaver-Burk, Hanes equation and Eadie-Hofstee approach of enzymatic kinetics, to evaluate several kinetic parameters, including maximum reaction velocity (V_{max}, mol.dm^{-3}.h^{-1}), Michaelis constant (K_M, mol.dm^{-3}), turnover number (K_{cat}, h^{-1}) and specificity constant (k_{cat}/ K_M, dm^3.mol^{-1}.h^{-1}). The turnover number (K_{cat}, h^{-1}) was obtained by dividing the maximum reaction velocity (V_{max}) by the concentration of the complex.

2.8. Structure Activity Relationship (SAR)

As biological or catalytic activity ranking cannot be determined by only one parameter, it depends on a combination of parameters, thus, there is an urgent need to derive SAR model to correlate the biological or catalytic activity of the subject compounds with their calculated chemical descriptors and find the most effective description model[20]. SAR statistical model was constructed by correlating the practical biological (MIC) or catalytic (K_{cat}) of the subject

compounds with their theoretical chemical descriptors (E_{HOMO}, E_{LUMO}, ΔE, χ, μ, η, σ, ω and Nu), using multiple linear regressions (MLR).

$$K_{cat} = \text{constant} + a_1 E_{HOMO} + a_2 E_{LUMO} + a_3 \Delta E + a_4 \chi + a_5 \mu + a_6 \eta + a_7 \sigma + a_8 \omega + a_9 Nu \quad (1)$$

$$MIC = \text{constant} + b_1 E_{HOMO} + b_2 E_{LUMO} + b_3 \Delta E + b_4 \chi + b_5 \mu + b_6 \eta + b_7 \sigma + b_8 \omega + b_9 Nu \quad (2)$$

3. Results and Discussion

3.1. Structure elucidation of the prepared ligands

Structure elucidation of the subject HN, HB and HI ligands is listed in the Supplementary information.

3.2. Structure elucidation of the prepared ternary complexes

3.2.1. Complex stoichiometry

Spectrophotometric study was carried out to determine the Fe(III):Ligand:co-ligand molar ratio of the target complexes [21], Supplementary information, Fig. (S4).

According to these results a ratio of 1:1:1 (Fe : Ligand : co-ligand) had been identified for all complexes suggesting the following reaction:

$$Fe^{3+}{}_{(aqs)} + HLigand + Hco\text{-}ligand = [Fe(HLigand)(Hco\text{-}ligand)]^{3+}$$

To find out the manner in which ligands bind to the metal ion, a FT-IR spectrum was analyzed.

3.2.2. Ligand binding mode with metal ion

IR spectra of the complexes were compared with that of bare ligands to determine the coordination sites that may be involved in chelation, Supplementary information, Figs. (S5, S6 and S7).

The azomethine group υ(-CH=N) stretching vibration of the HN ligand appeared at 1610 cm^{-1}, was shifted to lower wave numbers at 1551, 1585 and 1585 cm^{-1}, for FeNQ, FeNB and FeNI, respectively, which gave good indication for the participation of -CH=N in chelation with the metal ion [22,23].

The υ(C-O) appeared at 1250, 1234, 1248 and 1245 cm^{-1}, for the free HN, HQ, HB and HI ligands, respectively, was shifted to higher frequencies after complexation to appear at 1284, 1273 and 1287 cm^{-1} for FeNQ, FeNB and FeNI, respectively[24]. In addition, the phenolic υ(OH) vibration of the free HN, HQ, HB and HI ligands appeared at 3323, 3370, 3311 and 3191 cm^{-1}, respectively, was disappeared upon complexation[15]. These confirm the participation of the phenolic (-OH) of the HN, HQ, HB and HI ligands in coordination with metal ion after de-

protonation. The broad band above 3400 cm^{-1}, had been assigned to υ(OH) of coordinated water molecules.

The υ(-C=N) of the quinoline, benzimidazole and imidazole moiety appeared at ≈ 1588, 1574 and 1588 cm^{-1} in the bare in HQ, HB and HI co-ligands, respectively, which shifted to lower wave numbers upon coordination with the metal ion to appear at 1480, 1522 and 1545 cm^{-1} for FeNQ, FeNB and FeNI, respectively. This shift gave evidence for the participation of the (-C=N) of co-ligands in chelation with the metal ion.

Furthermore, new bands are found in the IR spectra of the complexes in the regions 525-565 and 420-453, which are assigned to υ(M-O) and υ(M-N), respectively[25].

These data indicate that the HN ligand participated as mono-negatively bi-dentate ligand through the azomethine nitrogen (-CH=N) and phenolic oxygen after de-protonation. While, the HQ, HB and HI co-ligands participated as mono-negatively bi-dentate co-ligand through the (-C=N) nitrogen and phenolic oxygen after de-protonation. Therefore, the formed complexes would be formulated as; $[Fe(ligand)(co\text{-}ligand)(H_2O)_n]^+$.

3.2.3. Conductivity measurements

The isolated complexes were insoluble in water but soluble in common organic solvents, e.g. ethanol, acetone, DMF and DMSO. The molar conductivity of the isolated complexes in ethanol was relatively low, indicating the non-electrolytic nature of the isolated complexes.

Moreover, according to the non-electrolytic nature of the Fe(III) complexes, it would be inferred that chloride ion coordinated to Fe(III) ion to satisfy the valence. The presence of Cl^- ion inside the coordination sphere of Fe(III) complexes was confirmed by reaction with $AgNO_3$, as precipitation of AgCl after acid dissociation of the subject complexes using conc. HNO_3. Therefore, the formed complexes would be formulated as; $[Fe(ligand)(co\text{-}ligand)(H_2O)_n(Cl)]$.

3.2.4. Coordinated and non-coordinated water molecules

The number of coordinated and non-coordinated water molecules in the Fe(III) complexes was determined through the thermal analysis of the complexes[26] undergo drying at ≈ 100-110 ºC, followed by heating at ≈ 200-210 ºC, the weight loss was evaluated after each step.

The percentage observed (calculated) weight loss in the first step was 6.69 (6.45), 6.17 (5.85), and 7.04 (7.35) %, for FeNQ, NiNB, and CuNI, respectively, suggested the elimination of two non-coordinated "water of hydration" molecules in the case of FeNQ, and FeNB, while three molecules in the case of FeNI complex.

In the next step (weight loss), the percentage observed (calculated) was 3.98 (3.63), 3.73 (3.11), and 2.04 (2.64) %, for FeNQ, FeNB, and FeNI, respectively, suggested the elimination of one coordinated water molecule in all the complexes. Therefore, the formed complexes would be formulated as $[Fe(L)(Q)(Cl)(H_2O)].2H_2O$, $[Fe(L)(B)(Cl)(H_2O)].2H_2O$ and $[Fe(L)(I)(Cl)(H_2O)].3H_2O$, for FeNQ, FeNB and FeNI complexes, respectively.

3.2.5. Effective magnetic moment and geometry of the Fe(III) complex

The structure geometry of the Fe(III) complexes would be elucidated from the magnetic susceptibility measurements. The susceptibility per gram atom of a paramagnetic metal ion in a particular compound was determined by measuring the molar susceptibility of the compound and applying diamagnetic corrections. The diamagnetic corrections would be determined by various methods, however Pascal's constants are more often used to calculate the corrections[27]. The measured gram magnetic susceptibility, X_g, of the complexes was utilized to calculate effective magnetic moment, $\mu_{eff} = 2.83 \times (((X_g \times \text{Mwt}) - (\text{diamagnetic correction})) \times T)^{0.5}$, in Bohr Magneton, where T is the absolute temperature (K)[17].

The measured μ_{eff} of FeNQ, FeNB, and FeNI complexes at room temperature were 1.907, 1.929 and 1.971 B.M, respectively, which would be attributed to one unpaired electron back to d^2sp^3 hybridization, suggesting a low spin octahedral geometry.

3.2.6. Electronic spectra

The electronic absorption spectra of Fe(III) complexes was recorded at room temperature using acetonitrile as solvent and were compared with that of bare ligands, Supplementary information, Figs. (S8, S9 and S10).

The free ligands exhibit absorption bands at (230, 310 & 380) for HN, at (260 & 350) for HQ, at (235 & 320) for HB and at (210 & 315) for HI. These bands can be attributed to $\pi \rightarrow \pi^*$ and $n \rightarrow \pi^*$ transition in the ligand moiety.

The observed shoulder spectral features of the Fe(III) complexes at 360, 320 and 340 nm, for FeNQ, FeNB and FeNI, respectively, would be assigned to $n \rightarrow \pi^*$. Additionally, the broad band observed at 490, 460 and 470 nm, for FeNQ, FeNB and FeNI, respectively, would be assigned to Cl-Fe charge transfer transition[28].

3.2.7. Powder X-ray diffraction studies

Though the synthesized metal complexes were soluble in some polar organic solvents like DMSO and DMF, crystals that are suitable for single crystal studies were not obtained. In order to

test the degree of crystallinity of the synthesized metal complexes, we obtained the powder X-ray diffraction pattern of Fe(III) complexes. The powder X-ray diffraction pattern of the complexes was scanned in the range 10-80^0 (2θ) at wave length 1.54 Å. The diffractogram and associated data depict the 2θ value for each peak, relative intensity and inter-planar spacing (d-values). In all the complexes, the trend of the curves decreases from maximum to minimum intensity indicating the amorphous nature of the complexes in the present metal–ligand formation.

Powder X-ray diffraction pattern of Fe(III) complex, Fig. (1), showed 17, 14 and 20 reflections for FeNQ, FeNB and FeNI complexes, respectively, with maxima at 2θ = 22.275°, 24.992° and 31.525°, corresponding to d-value 3.98 Å, 3.56 Å and 2.83 Å, respectively. The inter-planar spacing (d) had been calculated by using Bragg's equation; d = nλ/2sinθ. The calculated inter-planar d-spacing together with relative intensities with respect to most intense peak had been recorded and depicted in Supplementary information, Tables. (S1, S2 and S3).

For the Fe(III) complexes unit cell, calculations had been done for cubic symmetry from the entire peaks and $h^2+ k^2+ l^2$ values were determined. The observed inter-planar d-spacing values have been compared with the calculated ones and it was found to be in good agreement, Supplementary information, Tables. (S1, S2 and S3). The $h^2+ k^2+ l^2$ values of FeNQ and FeNB complexes showed the presence of forbidden number 7, while FeNI complex showed the presence of forbidden number 15 and 23. These indicate that the complexes may belong to hexagonal or tetragonal systems[24,29].

The particle size of these complexes was estimated from their PXRD patterns based on the highest intensity value compared to the other peaks using the well-known De-bye–Scherrer formula, D(the apparent particle size of the grains) = kλ/βcosθ; where; K is a constant (0.94 for Cu grid), λ is the X-ray wavelength used (1.5406 Å), θ is half the scattering angle (the Bragg diffraction angle), and β is the full-width at half-maximum (FWHM) of the X-ray diffraction line (additional peak broadening). The crystallite size of the FeNQ, FeNB and FeNI complexes was found to be 58.27, 23.61 and 204.41 nm, respectively, suggesting that the complexes are in a nano crystalline phase, Supplementary information, Table. (S4).

3.3. DFT calculations

3.3.1. Geometry optimization of the complexes

The Fe(III) mixed-ligand complexes were formulated as [Fe(Ligand)(co-ligand)(Cl)(H_2O)], in which the chloride and water molecules can be oriented in trans or cis binding mode to each other around the Fe(III) center, Fig. (2a,b). In the trans binding mode, the bulky organic ligands were in the same plane and are close to each other with high steric hindrance, Fig. (2a). While in

the optimized cis binding mode of the Fe(III) complexes, the bulky organic ligands were oriented perpendicular to each other around the Fe center , *Fig. (2b)*, this orientation decreases the steric hindrance. The calculated donor-acceptor bond lengths and bond angle for the cis- binding mode, are listed in *Table (1)*.

Table (1): Calculated selected bond lengths (Å) and bond angels (°) of the Fe(III) complexes.

bond length (Å)		**bond angel (°)**			
FeNQ					
Fe-N_{HN}	1.96	N_{HN}-Fe-N_{HQ}	175.59	N_{HQ}-Fe-H_2O	89.13
Fe-N_{HQ}	2.00	N_{HN}-Fe-O_{HQ}	92.57	O_{HQ}-Fe-H_2O	86.52
Fe-O_{HN}	1.86	N_{HN}-Fe-O_{HN}	92.61	O_{HQ}-Fe-O_{HN}	96.36
Fe-O_{HQ}	1.90	N_{HN}-Fe-Cl	89.34	O_{HQ}-Fe-Cl	167.87
Fe-Cl	2.37	N_{HN}-Fe-H_2O	93.74	O_{HN}-Fe-Cl	95.52
Fe-OH_2	2.03	N_{HQ}-Fe-O_{HQ}	84.26	O_{HN}-Fe- H_2O	172.91
		N_{HQ}-Fe-O_{HN}	84.72	Cl-Fe- H_2O	81.40
		N_{HQ}-Fe-Cl	94.40		
FeNB					
Fe-N_{HN}	1.98	N_{HN}-Fe-N_{HB}	177.72	N_{HB}-Fe-H_2O	88.44
Fe-N_{HB}	2.01	N_{HN}-Fe-O_{HB}	88.57	O_{HB}-Fe-H_2O	88.93
Fe-O_{HN}	1.85	N_{HN}-Fe-O_{HN}	92.01	O_{HB}-Fe-O_{HN}	96.43
Fe-O_{HB}	1.90	N_{HN}-Fe-Cl	85.13	O_{HB}-Fe-Cl	166.10
Fe-Cl	2.41	N_{HN}-Fe-H_2O	93.57	O_{HN}-Fe-Cl	96.16
Fe-OH_2	2.03	N_{HB}-Fe-O_{HB}	90.39	O_{HN}-Fe- H_2O	172.37
		N_{HB}-Fe-O_{HN}	86.10	Cl-Fe- H_2O	79.14
		N_{HB}-Fe-Cl	96.33		
FeNI					
Fe-N_{HN}	2.00	N_{HN}-Fe-N_{HI}	177.96	N_{HI}-Fe-H_2O	84.23
Fe-N_{HI}	2.01	N_{HN}-Fe-O_{HI}	84.81	O_{HI}-Fe-H_2O	88.49
Fe-O_{HN}	1.87	N_{HN}-Fe-O_{HN}	91.34	O_{HI}-Fe-O_{HN}	94.18
Fe-O_{HI}	1.88	N_{HN}-Fe-Cl	85.49	O_{HI}-Fe-Cl	164.40
Fe-Cl	2.39	N_{HN}-Fe-H_2O	95.43	O_{HN}-Fe-Cl	98.24
Fe-OH_2	2.05	N_{HI}-Fe-O_{HI}	93.17	O_{HN}-Fe- H_2O	172.93
		N_{HI}-Fe-O_{HN}	177.96	Cl-Fe- H_2O	80.30
		N_{HI}-Fe-Cl	84.81		

Energetically, cis- binding mode was found to be more stable than trans- mode for all complexes. The calculated energy difference was -7.76, -0.67 and -4.78 kcal/mol for FeNQ, FeNB and FeNI, respectively.

In order to perform a comparative study of the stability of the studied complexes, the Binding Energy (BE) or the complexation energy was calculated as follow[30]

$$E_{binding} = E_{complex} - (E_{Metal} + E_{primary\text{-}ligand(HN)} + E_{Secondary\ co\text{-}ligand} + E_{Cl} + E_{H2O})$$

The more negative binding energy corresponds to the most stable complex. From the calculated values one can notice that all complexes are more stable than their corresponding

ligands. And the order of the complexes stability is FeNQ (-439.56) > FeNB (-427.64) > FeNI (-418.61).

3.3.2. Frontier molecular orbital analysis

The HOMO as an electron donor, represents the ability to donate an electron, while, LUMO as an electron acceptor, represents the ability to obtain an electron. Both HOMO and LUMO are the main orbitals take part in chemical stability[31]. Whereas, the negative values of E_{HOMO} and E_{LUMO} point to the stability of the molecule. The larger HOMO energy suggested that the molecule is a decent electron donor and it proposed that its electron donation character is vital for the formation of a charge-transfer complex among the molecule and biological target. On opposing, the low HOMO energy values indicated that the molecule donating ability is weaker. The HOMO and LUMO energies of ligands and their complexes calculated by the DFT method are listed in *Table (2)*. Besides, the pictorial representation of their HOMO-LUMO distribution and their respective positive and negative regions is shown in *Fig. (3)*. Calculations of molecular orbital configuration indicated that HOMO and LUMO were delocalized through the whole molecule supporting the aromaticity among the phenyl skeleton. HOMO and LUMO orbitals for the complex structures were also delocalized all over the molecule, *Fig. (3)*.

Table (2): Calculated HOMO, LUMO, energy gap (ΔE), electronegativity (χ), Chemical hardness (η), Softness (σ), chemical potentials (μ), electrophilicity index (ω), and nucleophilicity (Nu), by eV unit, of the Fe(III) complexes.

	HOMO	**LUMO**	ΔE	η	σ	μ	χ	ω	Nu
FeNQ	-5.45	-2.43	3.03	1.51	0.33	-3.94	3.94	5.13	0.20
FeNB	-5.42	-2.51	2.91	1.46	0.34	-3.97	3.97	5.40	0.19
FeNI	-5.32	-2.49	2.83	1.42	0.35	-3.90	3.90	5.38	0.19

The HOMO-LUMO energy gap is correlated with various biological aspects like antibacterial, antioxidant and DNA binding aspects [32]. Selected quantum chemical parameters had been derived from E_{HOMO}, E_{LUMO}, and used to evaluate the chemical reactivity of the complexes. Specifically, ΔE, χ, μ, η, σ, ω, and Nu, descriptors had been calculated and summarized in *Table (2)*.

Other important parameter E_{LUMO} is related with electron accepting from appropriate molecule. If its energy is low, the molecule can accept electrons from the appropriate molecule and this result shows that chemical reactivity increases with decreasing of E_{LUMO}. Chemical reactivity

ranking should be given as follow: FeNB>FeNI>FeNQ. Accordingly, FeNB is the most reactive in gas phase.

Energy gap between LUMO and HOMO is important to determine the reactivity ranking due to the electron mobility. Smaller value of this parameter means that molecule is more reactive, thus, chemical reactivity increases with decreasing of ΔE values. According to ΔE, the reactivity ranking should be as follow: FeNI>FeNB>FeNQ. Accordingly, investigated FeNI is the most reactive in gas phase.

The other important parameters to explain the chemical reactivity ranking are hardness and softness. The biological activity tendencies of complexes towards appropriate molecules can be discussed with the hard–soft–acid–base (HSAB) approximation. The rule is that hard acids prefer to coordinate to hard bases and soft acids to soft bases. Biological structures such as the cell, enzyme, etc. are soft. Therefore, Soft complexes can interact easily with biological molecules than hard molecules. So, biological activity increased with the increasing softness and decreasing hardness values. The order of chemical hardness is FeNQ > FeNB > FeNI suggesting that FeNI is the most reactive.

Chemical potential is other important parameters to determine the chemical reactivity ranking. Chemical potential is directly proportional with Gibbs free energy and these parameters can be related with spontaneity. The chemical reactivity increases with decreasing of chemical potential, thus chemical reactivity ranking should be as follow: FeNB>FeNQ>FeNI, but the difference is insignificant.

Other important parameter is electrophilicity and nucleophilicity indexes. The electrophilicity index implies the ability of the electron accepting while nucleophilicity index displays the ability of electron donating. The chemical reactivity ranking as electrophile is FeNQ > FeNI > FeNB and vise-versa as nucleophile.

It can be noticed that reactivity cannot be determined through one descriptor, rather than it depends on a combination of these mentioned parameters. Thus, there is an urgent need to derive SAR model to correlate the biological activity of the investigated compounds with the calculated chemical descriptors and find the most effective description.

3.4. *In-vitro* antimicrobial Screening

The subject complexes exhibited high enhancement in their antimicrobial activity than the free ligands as can be seen in Table (3) and *Fig. (4)*. The increased in activity of the Fe(III) mixed-ligand complexes than their free ligands, would be explained on the basis of chelation theory[33,34,35]. This theory states that chelation reduces the polarity of the metal ion by the partial

sharing of its positive charge with donor groups and possible π-electron delocalization over the whole ring. This leads to increasing lipophilic character of the complex and penetration of the complex through the lipid layer of cell membrane. The complex may block the binding sites of microorganisms; consequently it disturbs the metabolism pathways and respiration process in the cell, and thus blocks the synthesis of proteins, which restricts further growth of the organism and resulting in the extinction of microorganisms.

Table (3): antimicrobial activities in terms of Diameter of inhibition zone in mm and minimum inhibition concentration (MIC) of HL and its complexes at 100 µg/ml.

	Anti-bacteria activity						**Anti-fungi activity**		
	E. coli (G^-)			**B. cereus (G^+)**			**Aspergillus fumigatus**		
	IZ	**MIC (µg/ml)**		**IZ**	**MIC (µg/ml)**		**IZ**	**MIC (µg/ml)**	
	(mm)	**MIC_{pr}**	**MIC_{calc}**	**(mm)**	**MIC_{pr}**	**MIC_{calc}**	**(mm)**	**MIC_{pr}**	**MIC_{calc}**
HN	6.30	75.50	75.48	6.20	77.50	77.53	6.70	67.50	67.49
HB	7.10	54.50	54.48	7.30	53.50	53.53	8.20	56.50	56.48
HI	7.60	57.50	57.48	8.00	56.50	56.53	8.30	54.50	54.49
HQ	6.90	65.50	65.48	6.80	65.50	65.53	7.40	65.50	65.49
NFeQ	14.50	25.50	25.48	15.30	27.50	27.52	16.40	26.50	26.49
NFeB	16.20	22.50	22.48	17.70	24.50	24.52	18.70	23.50	23.49
NFeI	16.20	23.50	23.48	17.00	25.50	25.52	17.90	24.50	24.49

Current investigated complexes showed better MIC values comparing with previously reported transition metal complexes against *E. coli* [36,37] and *B. cereus*[38,15].

3.5. Phenoxazinone synthase mimicking activity

Spectrophotometric scan for the coupling oxidation of OAP to Phz in the presence of Fe(III) complexes revealed a gradual increase in intensity of the absorption band at 430 nm, confirms the phenoxazinone synthase like activity, Fig. (5).

3.5.1. Kinetic investigation through several enzyme kinetic plots

The Michaelis-Menten model is the simplest and best-known approaches to catalyst kinetics. The Michaelis-Menten equation relates the reaction velocity to substrate concentration for a system, as follow;

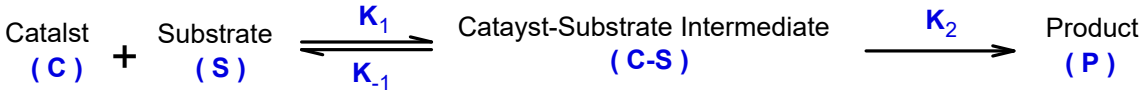

Biochemical reactions involving a single substrate are often assumed to follow Michaelis-Menten kinetics, $V = (V_{max} / (K_M + [S]))\times[S]$, which is an important tool for treating this type of saturation rate dependency on substrate concentration. Where, V_{max} (mol.dm^{-3} h^{-1}) represents the maximum rate achieved by the system, at saturating substrate concentration. K_M (mol.dm^{-3}) is the Michaelis constant and it is equal to the substrate concentration at which the reaction rate is half of V_{max}. Michaelis-Menten model is used to relate the rate of enzymatic reactions (V) to the concentration of substrate ([S]), Supplementary information, Figs. (S11.a, S12.a and S13.a).

Linearization of Michaelis-Menten equation produces a double reciprocal Lineweaver-Burk plot, $(1/V) = (1/V_{max}) + ((K_M/V_{max})\times(1/[S]))$, Supplementary information, Figs. (S11.b, S12.b and S13.b), that is used to analyze a variety of kinetic parameters, e.g. V_{max} and K_M.

On the other hand, rearrangement of Michaelis-Menten equation gives Hanes equation, $([S]/V) = K_M/V_{max} + (1/V_{max})\times[S]$. In this case, the ratio of the substrate concentration (S) to the reaction rate (V) is plotted against substrate concentration ([S]), Supplementary information, Figs. (S11.c, S12.c and S13.c).

Eadie-Hofstee equation, $V = V_{max} + K_M\times(V/[S])$, is sometimes used in biochemistry for a graphical representation of enzyme kinetics. Here reaction rate (V) is plotted as a function of the ratio between reaction rate (V) and substrate concentration ([S]), Supplementary information, Figs. (S11.d, S12.d and S13.d)**.**

All these enzyme kinetic plots were used to evaluate several kinetic parameters, including turnover number (K_{cat}, h^{-1}) and specificity constant (k_{cat}/K_M , mol^{-1}.dm^3.h^{-1}), Table (4). k_{cat} was defined as the maximum number of catalytic conversions of substrate molecules per unit time that a single catalytic site will execute for a specific enzyme concentration. k_{cat}/K_M is a measure of how efficiently a catalyst converts substrates into products. This ratio is a useful index for measuring the substrate specificity of catalyst. The higher k_{cat}/K_M, the more the enzyme prefers that substrate.

Table (4): Kinetic parameters for the oxidation of OAPH catalyzed by the synthesized Fe(III) complexes in acetonitrile.

	V_{max} (mol.dm^{-3} h^{-1})	**K_{cat} (h^{-1}) $K_{cat\ (practical)}$**	**$K_{cat\ (calculated)}$**	**K_M (mol.dm^{-3})**	**k_{cat}/K_M (mol^{-1}.dm^3.h^{-1})**
NFeQ	6.98 x 10^{-4}	209.53	209.52	3.61 x 10^{-3}	5.81 x 10^4
NFeB	5.73 x 10^{-4}	171.82	171.81	4.16 x 10^{-3}	4.13 x 10^4
NFeI	5.25 x 10^{-4}	157.58	157.57	3.74 x 10^{-3}	4.22 x 10^4

3.5.2. Mechanistic pathway of catalytic activity

Based on the literature survey[39,40,41,42,43,44,45,46,47], a tentative catalytic cycle for the formation of the phenoxazinone chromophore was shown in Scheme (2). Initially, OAP forms adduct with complexes replacing the monodentate chloride ligand. This results in the formation of OAP radical by the reaction with molecular dioxygen regenerating complexes. In the next step, the OAP radical may be oxidized to o-benzoquinone monoamine, which, in turn, may be converted to Phz by the reaction with dioxygen and OAP [19,48].

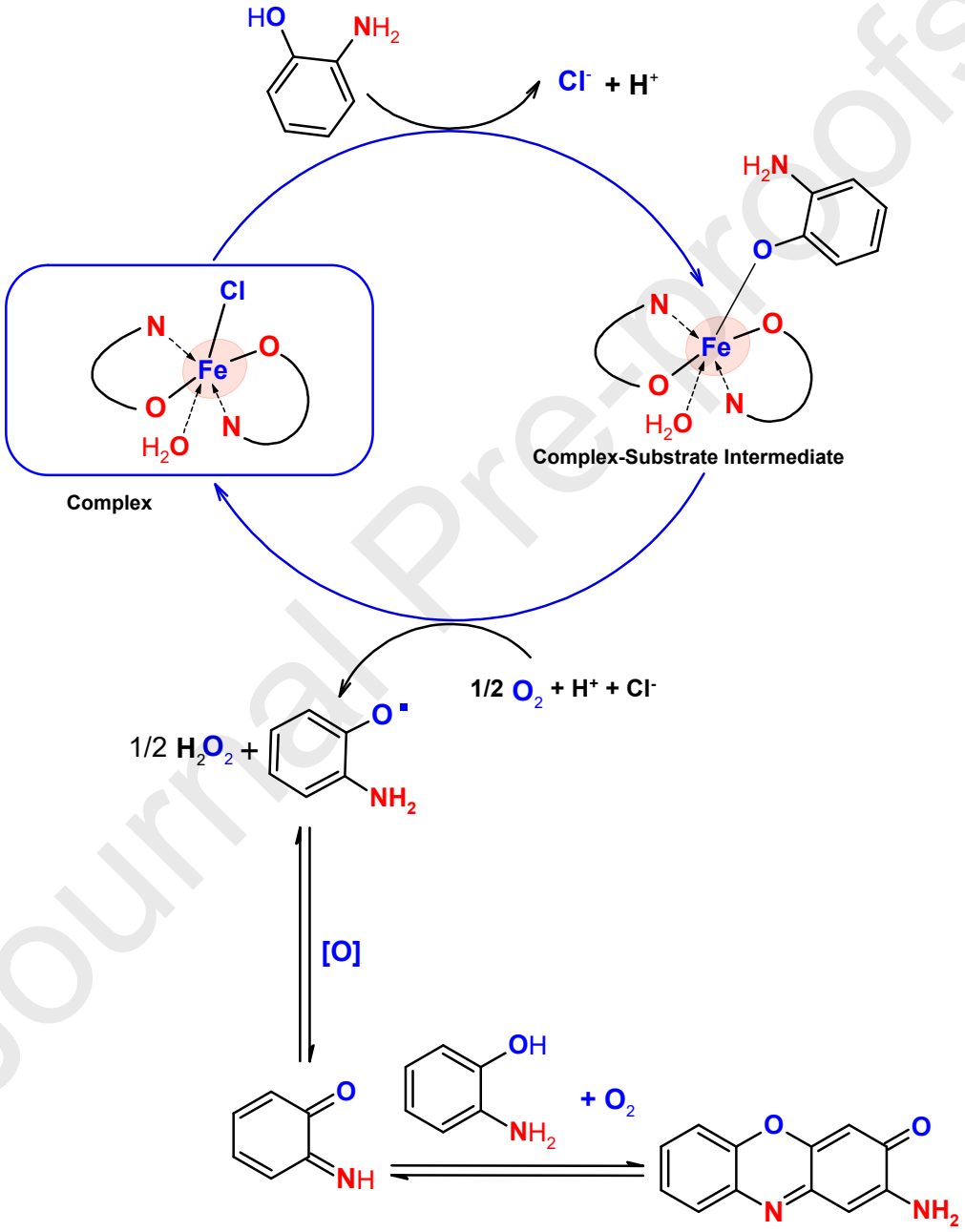

Scheme (2): Tentative mechanistic pathway for the coupling oxidation of OAP to Phz.

3.5.3. Comparative study

Transition metal complexes were wildly reported as being influential in the catalytic conversion of OAP to Phz[49]. A comparison was made between our synthetized complexes with other reported transition metal complexes. Noticeable differences in K_{cat} were observed, Table (5). K_{cat} of the recent Fe(III) complexes was found to be high comparing with other complexes indicating that the synthesized Fe(III) complexes will be an effective catalyst for OAP oxidation reaction.

Table (5): A comparison of turnover number (K_{cat}) values of some complexes available in the literature for the conversion of o-aminophenol to the corresponding phenoxazinone.

	Complex	K_{cat} (h^{-1})	Reference
1	$[Cu(L)_2](ClO_4)_2$	360.00	[50]
2	**FeNQ**	**209.53**	**This work**
3	$[FeLCl]_2$	196.18	[41]
4	**FeNB**	**171.82**	**This work**
5	**FeNI**	**157.58**	**This work**
6	$[Mn(HL)_2](ClO4)_2$	138.62	[51]
7	$[FeCl_2(L^5)]$	137.00	[52]
8	$[Mn(HL)(N(CN)_2)(H_2O)_2](ClO_4)$	64.07	[51]
9	$[Fe(L^1)Cl_3]$	56.00	[53]
10	$[Co(L)(N_3)_2]$	54.00	[54]
11	$[Co(L^2)(N_3)_3]$	33.26	[55]
12	$[Co(L^3)(N_3)_3]$	33.12	[55]
13	$[\{FeL(4,4'\text{-byp})ClO_4\}]_n$	32.36	[41]
14	$[Co_2(L^6)_2(\mu\text{-}O_2)](ClO_4)_4 \cdot 2CH_3CN$	30.09	[56]
15	$[Mn(L^2)Cl_2]$	27.32	[57]
16	$[Mn(L^4)Cl_2]\ H_2O$	26.32	[58]
17	$[Co(L^2)_2(\mu\text{-}O_2)](ClO_4)_4$	23.04	[56]
18	$[Mn(Br_4Cat)(Br_3pyCat)(py)_2]$	22.39	[59]
19	$[Ni(L)_2](ClO_4)_2$	21.40	[50]
20	$[Zn(L)_2](ClO_4)_2$	17.00	[50]
21	$[Co_2(amp)_2(\mu\text{-}imp)_2Cl_2]Cl_2 2H_2O$	13.75	[60]
22	$[Co(L^1)Cl(H_2O)]ClH_2O$	13.68	[61]
23	$[LCo(L')_2]ClO_4$	11.48	[49]
24	$[Mn(L^2)Cl_2]$	9.66	[58]
25	$[Mn(L^3)Cl_2]$	8.20	[58]
26	$[Co(L^1)(NCS_2)]$	7.38	[61]
27	$[Co(L^4)(H_2O)](ClO_4)_2$	6.37	[56]
28	$[Co(L^2)(Cl)_2]$	4.10	[51]
29	$[Co(L^3)(CH_3CN)](ClO_4)_2$	3.36	[56]
30	$[Mn(6'Me_2indH)(H_2O)_2(CH_3CN)](ClO_4)_2$	2.93	[62]

3.6. Structure-activity relationship (SAR)

Biological or catalytic activity of molecules can be evaluated through experimental and computational correlation[63,64,65].

The aim of the present SAR analysis was to correlate the experimental biological or catalytic activity of the investigated compounds with their quantum chemical descriptors and find the most effective description model. The multiple linear regression (MLR) was applied to develop a best relationship between the dependent variable, K_{cat} or MIC, with independent variables (chemical descriptors, E_{HOMO}, E_{LUMO}, ΔE, η, σ, μ, ω, and Nu).

The theoretical correlation formula was derived for phenoxazinone synthase mimicking activity (equation (3)), *E. coli* (G^-) (equation (4)), *B. cereus* (G^+) (equation (5)), and *A. fumigates* (equation (6)).

$$K_{cat} = - 86.63 - 165.30\, E_{HOMO} - 118.06\, \omega \quad (3)$$

$$MIC = -1092.78 - 5661.18E_{HOMO} - 6048.33E_{LUMO} + 1702.78\sigma + 11135.10\mu - 247.00\omega + 776.55Nu \quad (4)$$

$$MIC = -997.92 - 5861.27E_{HOMO} - 6262.79E_{LUMO} + 1610.21\sigma + 11554.00\mu - 248.91\omega + 707.86Nu \quad (5)$$

$$MIC = -824.71 - 4310.36E_{HOMO} - 4549.71E_{LUMO} + 1461.73\sigma + 8439.13\mu - 193.87\omega + 364.20Nu \quad (6)$$

To investigation the validity of derived formula, predicted MIC and K_{cat} values were compared with actual values, *Tables (5 and 6.)*, which, showed excellent agreement.

Additionally, a cross validation squared coefficient, $Q^2 = 1 - (\sum(Property_{pred.} - Property_{exp.})^2 / \sum(Property_{exp.} - Property_{mean.})^2)$, was calculated for evaluate the prediction power of the proposed model. Where; $Property_{pred.}$, $Property_{exp.}$, and $Property_{mean}$, are the predicted, experimental and mean values of the target property, MIC and K_{cat}.

Q^2 was found to be 0.99, 1.00, 1.00, and 1.00, for the investigated compounds against, phenoxazinone synthase mimicking activity, *E. coli* (G^-), *B. cereus* (G+), and *A. fumigatus*, respectively, which indicated excellent prediction power of the proposed SAR model, *Tables (4 and 5)*.

4. Conclusion

Three Fe(III) mixed-ligand complexes with a phenol-based Schiff base as the primary ligand, and N-containing heterocyclic ring as the secondary one had been synthesized and characterized. DFT calculations were performed to confirm the proposed geometry and estimate the electronic structure properties. The results indicated that the complexes adapted a distorted octahedral geometry. The *in-vitro* antimicrobial activity showed that the Fe(III) complexes exhibited higher inhibition against selected tested microorganisms compared to the free ligands. Furthermore, the complexes were found to be active towards phenoxazinone synthase mimicking

activity. The mimicking activity was assessed by following conventional Michaelis-Menten enzymatic kinetics. Kinetic studies of the catalytic cycles had been performed in detail using a variety of enzyme kinetics plots to evaluate different kinetic parameters, including the specificity constant. In addition, SAR model showed an excellent correlation between the experimental biological (MIC) and catalytic activity (K_{cat}) with the calculated quantum chemical descriptors.

References

Declaration of interests

☒ The authors declare that there is no Conflict of Interest of the results of the manuscript with any other third party.

Declaration of interests

☒The authors declare that they have no known competing financialinterestsor personal relationships that could have appeared to influence the work reported in this paper.

☐The authors declare the following financial interests/personal relationships which may be considered as potential competing interests:

Design and Synthesis of Three Fe(III) Mixed-ligand Complexes: Exploration of Their Biological and Phenoxazinone Synthase Like Activities

Mohammed Ismael*, Abdel-Mawgoud M. Abdel-Mawgoud, Mostafa K. Rabia and Aly Abdou

Chemistry Department, Faculty of Science, Sohag University, Sohag 82524, Egypt

Graphical Abstract

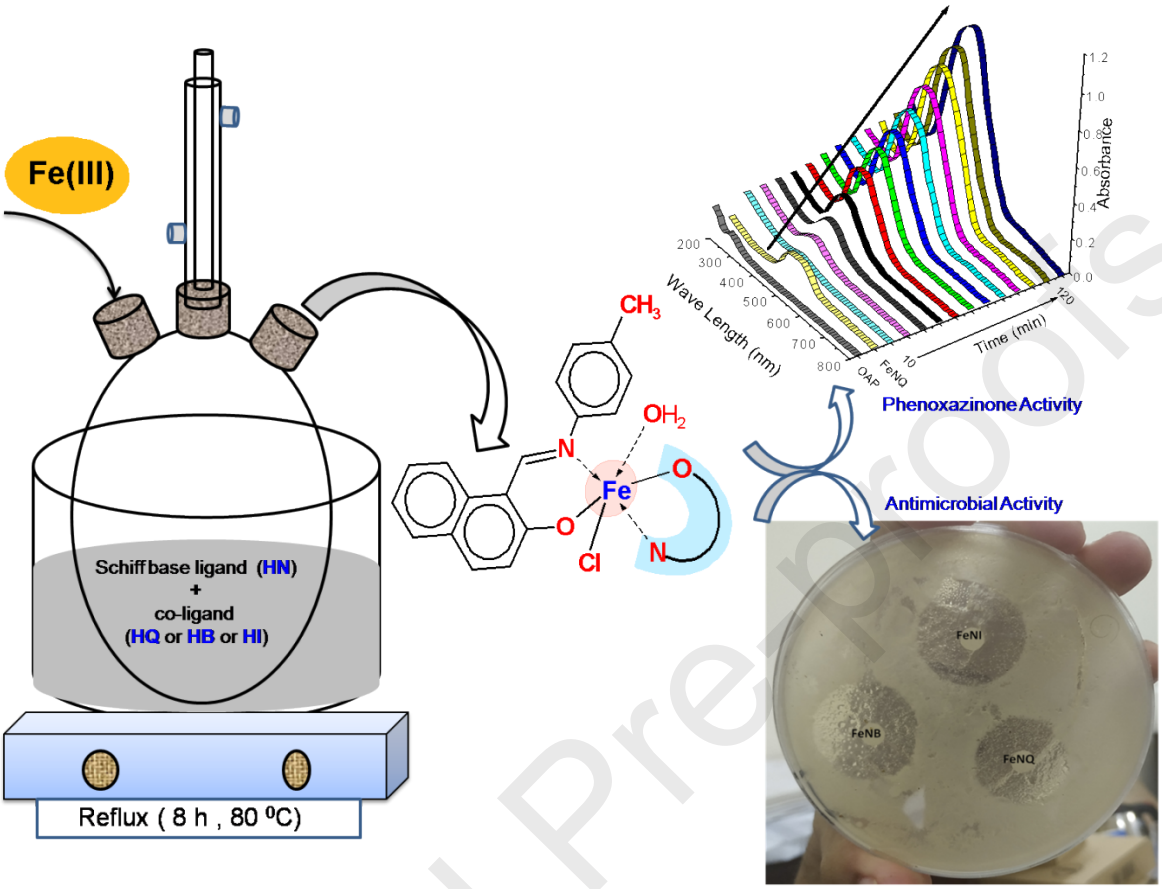

Design and Synthesis of Three Fe(III) Mixed-ligand Complexes: Exploration of Their Biological and Phenoxazinone Synthase Like Activities

Mohammed Ismael*, Abdel-Mawgoud M. Abdel-Mawgoud, Mostafa K. Rabia and Aly Abdou

Chemistry Department, Faculty of Science, Sohag University, Sohag 82524, Egypt

Highlights

- Three Fe(III) mixed-ligand complexes involving phenol-based Schiff-base ligand and N-containing heterocyclic ring have been synthesized and characterized.
- DFT calculations were performed to provide deep understanding of the complexes properties.
- The complexes showed a promising antibacterial and antifungal activity

- Phenoxazinone synthase mimicking activity was explored.
- Structure activity relationship (SAR) for these complexes had been derived.

List of figures

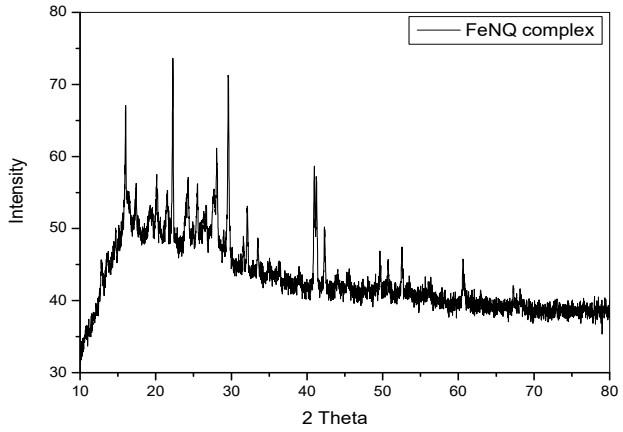

a)

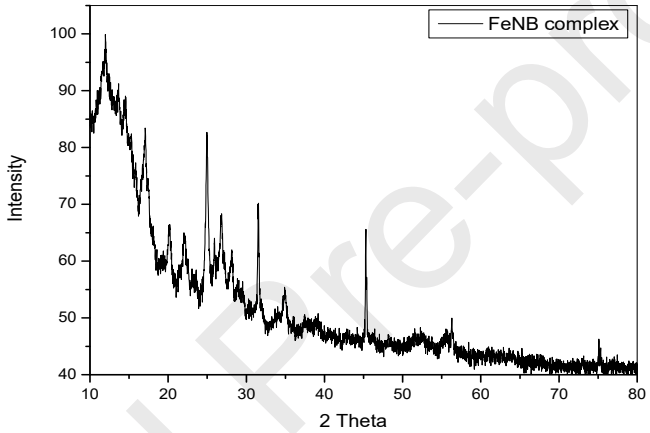

(b)

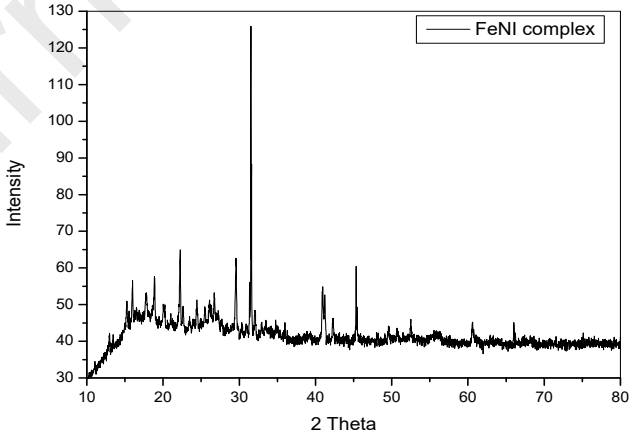

(c)

Fig. (1): Powder XRD spectrum of (**a**) FeNQ, (**b**) FeNB, and (**c**) FeNI, complexes.

(a). Trans-FeNQ complex

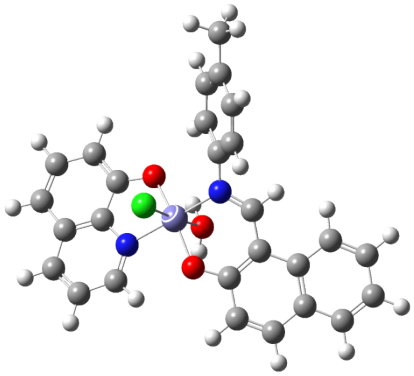

E_{Total} = - 951073.84 Kcal/mol

(b). Trans-FeNB complex

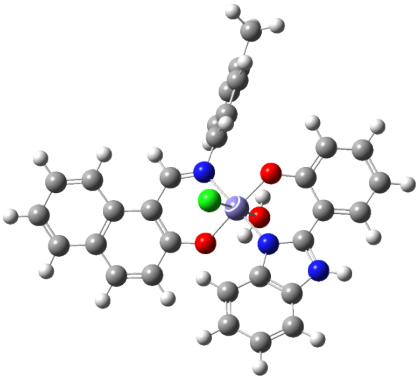

E_{Total} = - 1082200.64 Kcal/mol

(c). Trans-FeNI complex

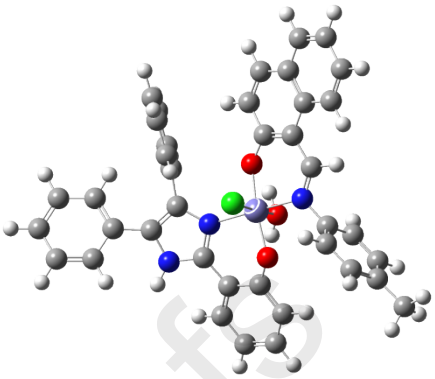

E_{Total} = - 1275725.51 Kcal/mol

(d). Cis-FeNQ complex

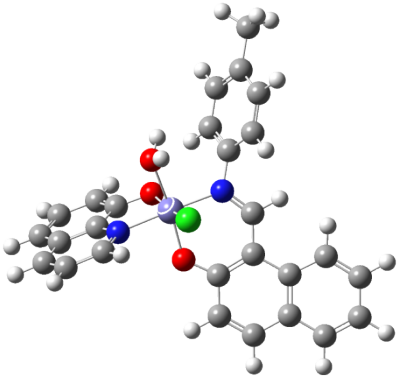

E_{Total} = - 951081.60 Kcal/mol

(e). Cis-FeNB complex

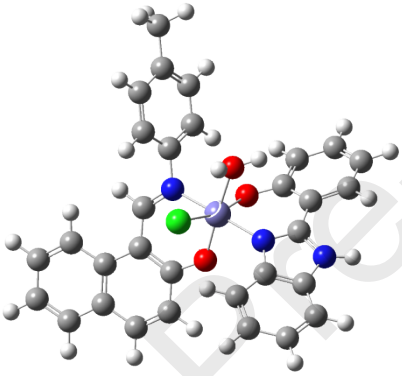

E_{Total} = - 1082201.32 Kcal/mol

(f). Cis-FeNI complex

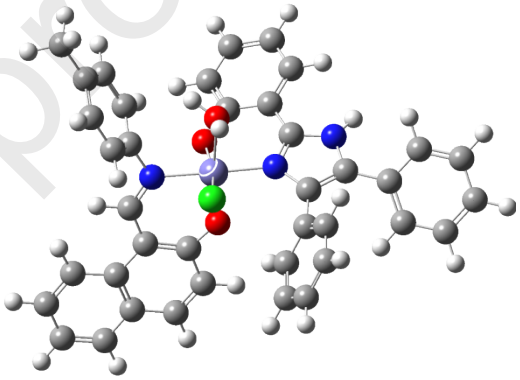

E_{Total} = - 1275730.288 Kcal/mol

Fig. (2): Optimized structures of **(a)** FeNQ, (**b**) FeNB, and (**c**) FeNI complexes.

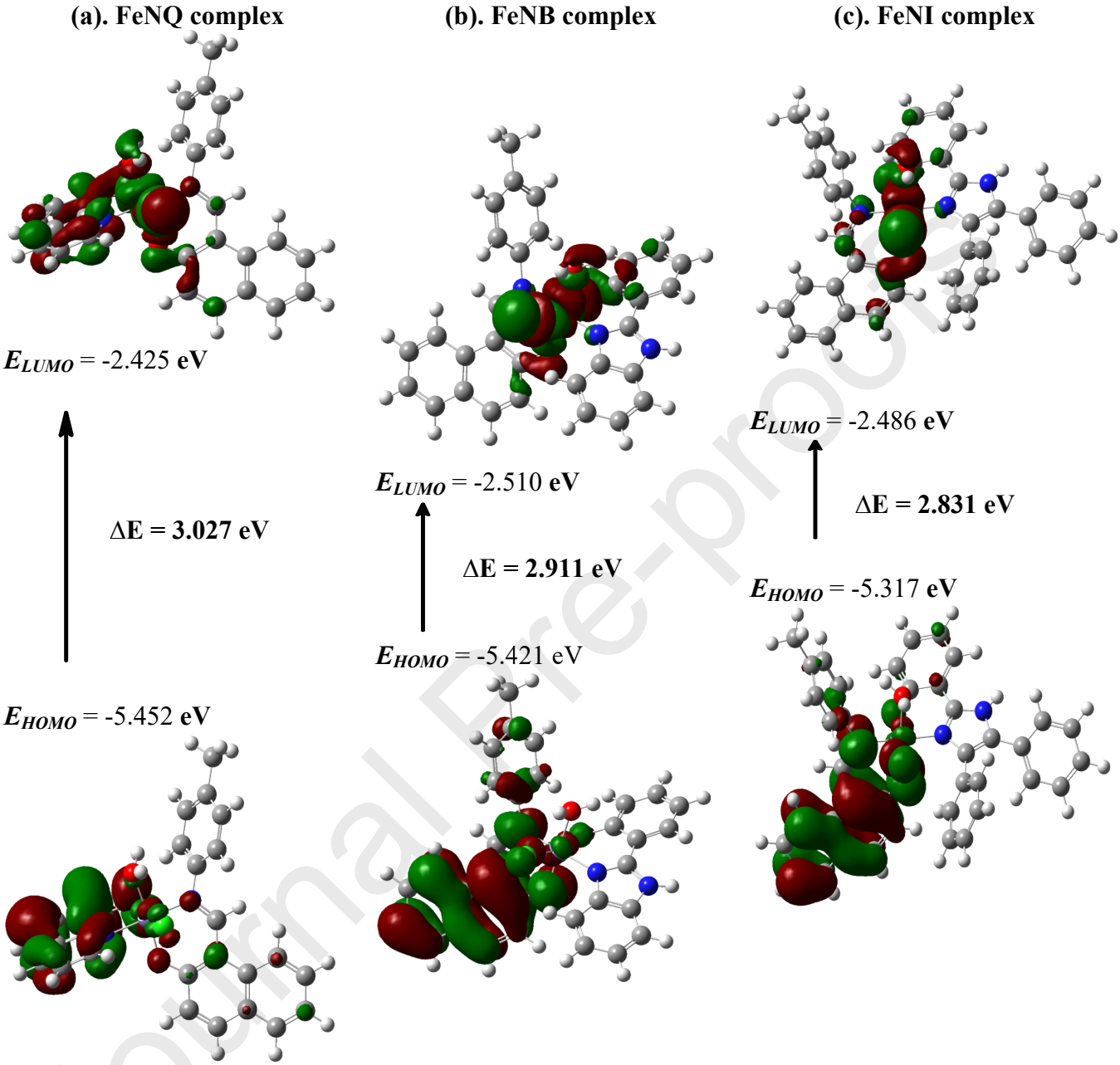

Fig. (3): Calculated HOMO and LUMO of (**a**) FeNQ, (**b**) FeNB, and (**c**) FeNI complexes.

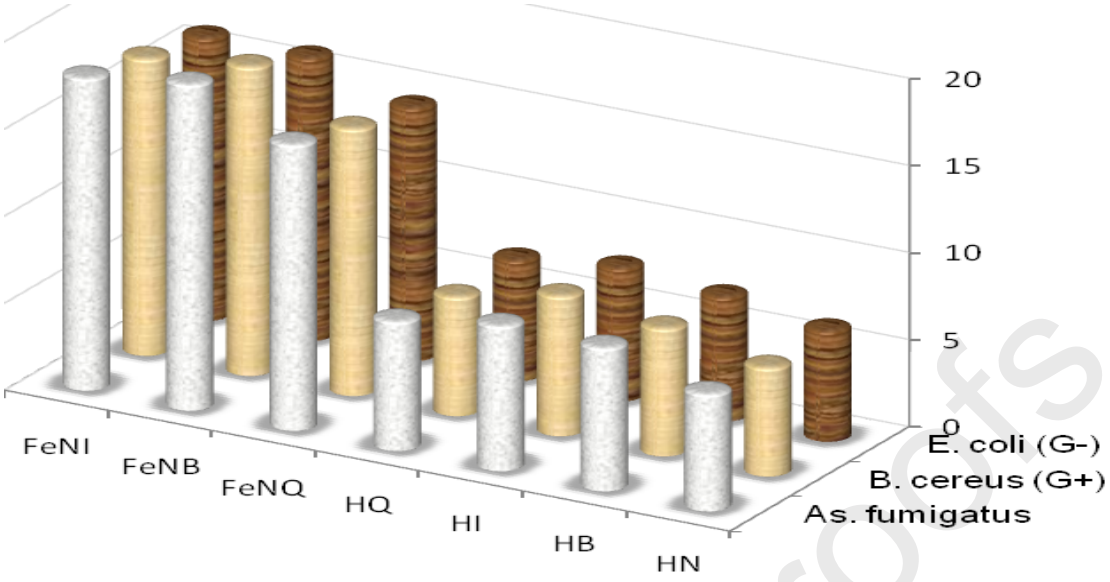

(a)

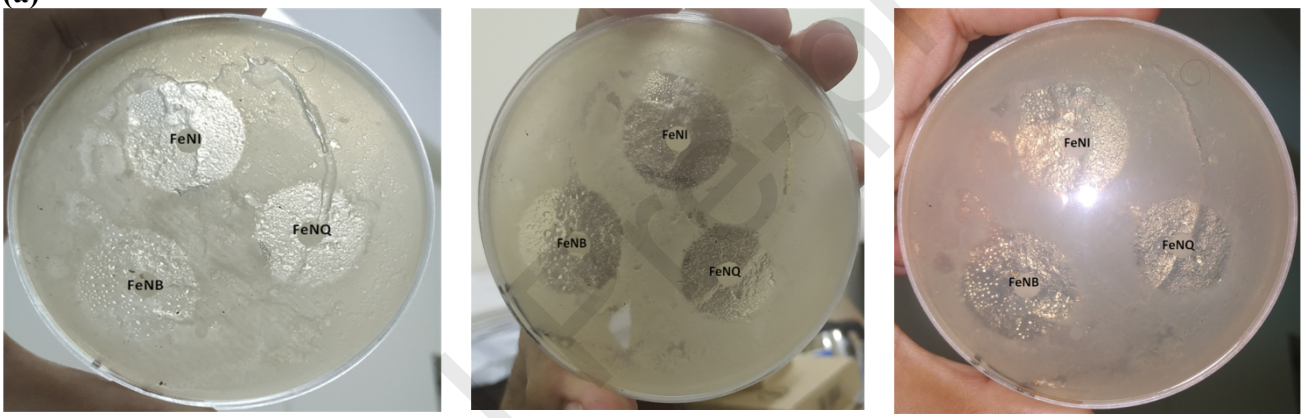

(b) **(c)** **(d)**

Fig. (4): (**a**) Antimicrobial activity of the free ligands and their Fe(III) complexes in term of inhibition zone diameter (IZ, mm) at 100 µg/ml, inhibition zone diameter of the Fe(III) complexes against (**b**) E. coli (G-), (**c**) B. cereus (G-) and (**d**) Aspergillus fumigates.

(a). FeNQ complex

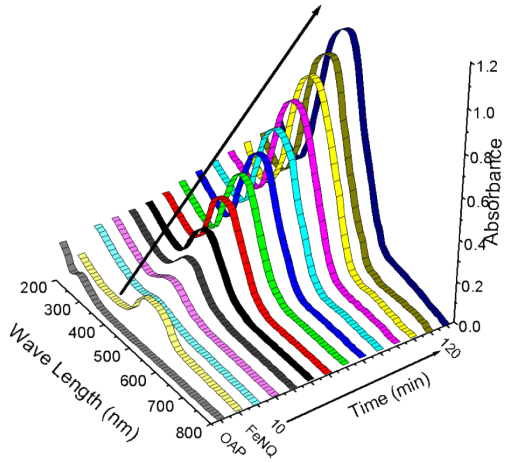

(b). FeNB complex

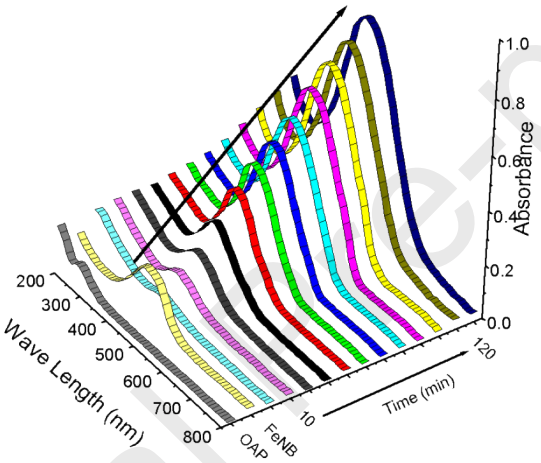

(c). FeNI complex

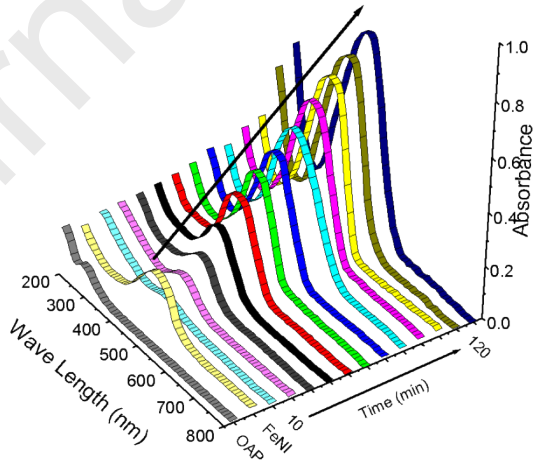

Fig. (5): Time resolved UV-Vis spectral profiles indicating the increment of Phz peak upon addition of 12×10^{-2} M OAP to 10^{-5} M of (a) FeNQ, (**b**) FeNB and (**c**) FeNI complexes.

[1] Hanan F. Abd El-Halim, Gehad G. Mohamed, Eman A.M. Khalil, Journal of Molecular Structure, 1146 (**2017**) 153-163

[2] G. Sasikumar, S. Arulmozhi, A . Ashma, A . Sudha, S.J. Askar ali, Journal of Molecular Structure, 1187 (**2019**) 108 -12 0

[3] Y. Bansal, O. Silakari, Bioorg. Med. Chem., 20 (**2012**) 6208-6236

[4] S. Baroniya, Z. Anwer, P. K. Sharma, R. Dudhe, N. Kumar, Der Pharmacia Sinica, 1 (**2010**) 172-182.

[5] R. V. Shingalapur, K. M. Hosamani, R. S. Keri, Eur. J. Med. Chem., 44 (**2009**) 4244-4248.

[6] A. Puratchikodya, M. Doble, Bioorg. Med. Chem., 15 (**2007**) 1083-1090.

[7] R. V. Shingalapur, K. M. Hosamani, R. S. Keri, M. H. Hugar, Eur. J. Med. Chem., 45 (**2010**) 1753-1759

[8] G. Navarrete-Vázquez, S. Hidalgo-Figueroa, M. Torres-Piedra, J. Vergara-Galicia, J. C. Rivera-Leyva, S. Estrada-Soto, I. León-Rivera, B. Aguilar-Guardarrama, Y. Rios-Gómez, R. Villalobos-Molina, M. Ibarra-Barajas, Bioorg. Med. Chem., 18 (**2010**) 3985-3991.

[9] J. Pandey, V. K. Tiwari, S. S. Verma, V. Chaturvedi, S. Bhatnagar, S. Sinha, A. N. Gaikwad, R. P. Tripathi, Eur. J. Med. Chem., 44 (**2009**) 3350-3355.

[10] M. Tonelli, M. Simone, B. Tasso, F. Novelli, V. Boido, F. Sparatore, G. Paglietti, S. Pricl, G. Giliberti, S. Blois, C. Ibba, G. Sanna, R. Loddo, P. La-Colla, Bioorg. Med. Chem., 18 (**2010**) 2937-2953

[11] H. A. Saadeh, I. M. Mosleh, M. M. El-Abadelah, Molecules, 14 (**2009**) 2758-2767.

[12] S. Indira, G. Vinoth, M. Bharathi, S. Bharathi, A. K. Rahiman, K. S. Bharathi, Inorganica Chimica Acta, 495 (**2019**) 118988

[13] P.J. Hay, W.R. Wadt., J. Chem. Phys. 82 (**1985**) 270–283

[14] M. J. Frisch, G. W. Trucks, H. B. Schlegel, G. E. Scuseria, M. A. Robb, J. R. Cheeseman, et al. Gaussian 09, Revision B.01. Wallingford CT: Gaussian Inc.; **2016**

[15] M. Ismael, A. Abdou and A. M. Abdel-Mawgoud, Zeitschrift für anorganische und allgemeine Chemie, 644 (**2018**) 1203-1214.

[16] M. Hakimi, M. Alikhani, M. Mashreghi, N. Feizi, H. Raeisi, Y. Mirzai, V. Eigner, M. Dusek, Journal of Molecular Structure, 1186 (**2019**) 355-361.

[17] A. M. Abd-Mawgoud, M. Ismael, A. Abdou, J. Pharm. Appl. Chem., 3 (**2017**) 259-266.

[18] P. Murray, E. Baron, M. Pfaller, F. Tenover, R. Yolken, (**1995**). Manual of Clinical Microbiology, 6th Edn., ASM Press, Washington DC.

[19] K. Ghosh, M. G.B. Drew, S. Chattopadhyay, Inorganica Chimica Acta 482 (**2018**) 23–33.

[20] K. Sayin , D. Karakaş, Spectrochimica Acta Part A: Molecular and Biomolecular Spectroscopy. 188 (**2018**) 537–546.

[21] M. Ahmad, R. Narayanaswamy, Pertanika J. Sci. & Technol. 13 (**2005**) 43- 60

[22] K. Singh and R.Thakur, Eur. Chem. Bull., 5 (**2016**) 193-201.

[23] S. M. Abdallah, M. A. Zayedb, G. G. Mohamed, Arabian Journal of Chemistry, 3 (**2010**) 103–113

[24] G.Y. Nagesh, B.H.M. Mruthyunjayaswamy, Journal of Molecular Structure 1085 (2015) 198–206

[25] N.T. Madhu, P.K. Radhakrishnan, M. Grunert, P. Weinberger, Linert W. Thermochimica Acta, 407 (**2003**) 73-84

[26] R. R. Zaky**,** T. A**.** Yousef, *J. Mol. Struct.,* 1002 (**2011**) 76-85

[27] G. A. Bain, J. F. Berry, J. Chem. Educ., 85 (**2008)** 532-536

[28] L. Abane-Merzouk, A. Adkhis, S. Terrachet-Bouaziz, M. Makhloufi-Chebli, Journal of Molecular Structure, 1186 (**2019**) 413-422

[29] Vivekanand D. B. and Mruthyunjayaswamy B. H. M., Asian J. Research Chem. 6 (**2013**) 35-46

[30] N. T. Rahmouni, N. Bensiradj, S. A. Megatli, S. Djebbar, O. B. Baitich, Spectrochimica Acta Part A: Molecular and Biomolecular Spectroscopy, 213 (**2019**) 235–248

[31] A. Fekri, R. Zaky, Journal of Organometallic Chemistry 818 (**2016**) 15 - 27

[32] N. Pravin, G. Kumaravel, R. Senthilkumar, N. Raman, Appl Organom etal Chem., 31 (**2017**) 2739-2756

[33] M. N. Uddin, D. A. Chowdhury, M. T. Islam, F. Hoque, *Orbital*: *Electron*. *J. Chem*., 4 (**2012**) 273–287.

[34] M. Ikram, S. Rehman, A. Faiz, S. Saeed-ur-Rehman, *Bull. Chem. Soc. Ethiop.,* 24 **(2010)** 201-207.

[35] T. O. Aiyelabola, I. A. Ojo, A. C. Adebajo, G. O. Ogunlusi, O. Oyetunji, E. O. Akinkunmi, A. O. Adeoye, *Adv. Biol. Chem.,* 2 **(2012)** 268-273.

[36] D. H. Nakahata, M. A. Ribeiro, P. P. Corbi, D. Machado, M. Lancellotti, W. R. Lustri, A. M. da Costa Ferreira, A. L.B. Formiga, Inorganica Chimica. Acta, 458 (**2017**) 224-232

[37] J. Valentová, S. Varényi, P. Herich, P. Baran, A. Bilková, J. Kožíšek, L. Habala, Inorganica Chimica. Acta, 480 (**2018**) 16-26

[38] A. P. Gulya, K. S. Lozan-Tyrshu, V. I. Tsapkov, Yu. M. Chumakov, E. Zhanno, V. F. Rudik, Russian Journal of General Chemistry, 83 (**2013**) 530–537

[39] Kousik Ghosh, Abhisek Banerjee, Antonio Bauza, Antonio Frontera, Shouvik Chatt opadhyay, RSC Adv., 8 (**2018**) 28216–28237

[40] Nandita Sarkar, Klaus Harms, Shouvik Chattopadhyay, Polyhedron, 141 (**2018**) 198–207

[41] Sourav Chatterjee, Dipankar Sukul, Priyabrata Banerjee, Jaydeep Adhikary, Inorganica Chimica Acta 474 (**2018**) 105–112

[42] Snehasish Thakur, Nandita Sarkar, Michael G.B. Drew, Antonio Bauzá, Antonio Frontera, Shouvik Chattopadhyay, Polyhedron 142 (**2018**) 83–92

[43] Kousik Ghosh, Klaus Harms, Shouvik Chattopadhyay, ChemistrySelect, 2 **(2017)** 8207 – 8220

[44] Nandita Sarkar, Klaus Harms, Antonio Bauza´, Antonio Frontera, Shouvik Chattopadhyay, ChemistrySelect, 2 (**2017**) 2975 – 2984

[45] Kousik Ghosh, Klaus Harms, Shouvik Chattopadhyay, Polyhedron 123 (**2017**) 162–175

[46] Adhikary, J.; Chakraborty, A.; Dasgupta, S.; Chattopadhyay, S.K.; Kruszynski, R.; Trzesowska Kruszynska, A.; Stepanović, S.; Gruden-Pavlović, M.; Swart, M.; Das, D., Dalton Trans. 45 **(2016)** 12409-12422

[47] Kousik Ghosh, Sumit Roy, Anindya Ghosh, Abhisek Banerjee, Antonio Bauzá, Antonio Frontera, Shouvik Chattopadhyay, Polyhedron 112 (**2016**) 6–17

[48] Akhtaruz Zaman, Samim Khan, Basudeb Dutta, Sobhy M. Yakout, Shebl S. Ibrahim, Mohammad Hedayetullah Mir, j. coordination chemistry, 72 (**2019**) 2362–2375

[49] M. Mahato, D. Mondal, H.P. Nayek, Chemistry Select, 1 (**2016**) 6777 - 6782

[50] Arnab Chatterjee, Sumitava Khan, Rajarshi Ghosh, Polyhedron, **(2019)**114151

[51] J. Adhikary, A. Chakraborty, S. Dasgupta, S.K. Chattopadhyay, R. Kruszynski, A. Trzesowska-Kruszynska, S. Stepanović, M. Gruden-Pavlović, M. Swart, D. Das, Dalton Trans., 45 (**2016**) 12409

[52] M. Szávuly, R. Csonka, G. Speier, R. Barabás, M. Giorgi, J. Kaizer, J. Mol. Catal. A Chem., 392 (**2014**) 120

[53] R. Bakshi, R. Kumar, P. Mathur, Cat. Comm., 17 (**2012**). 140

[54] A. Panja, N.C. Jana, P. Brandão, New J. Chem., 41 (**2017**) 9784

[55] A. Panja, M. Shyamal, A. Saha, T.K. Mandal, Dalton Trans., 43 (**2014**) 5443

[56] A. Panja, Dalton Trans., 43 (**2014**) 7760-7770

[57] A. Panja, RSC Advances, 4 **(2014)** 37085–37094;

[58] A. Panja, Polyhedron, 79 (**2014**) 258-268

[59] A. Panja, N.Ch. Jana, M. Patra, P. Brandão, C.E. Moore, D.M. Eichhorn, A. Frontera, J. Mol. Catal. A Chem., 412 (**2016**) 56

[60] A. Panja, P. Guionneau, Dalton Trans., 42 (**2013**) 5068

[61] A. Panja, Polyhedron, 80 (**2014**) 81-89

[62] J. Kaizer, G. Baráth, R. Csonka, G. Speier, L. Korecz, A. Rockenbauer, L. Párkányi, J. Inor. Biochem., 102 (**2008**) 773.

[63] K. Sayin, D. Karakaş, Spectrochim. Acta A Mol. Biomol. Spectrosc., 193 (**2018**) 147-155.

[64] K. Sayin, D. Karakaş, J. Clust. Sci., 28 (**2017**) 3075–3086

[65] K. Sayin, D. Karakaş, Spectrochim. Acta A Mol. Biomol. Spectrosc., 188 (**2018**) 537–546.